CrossMark

A Constitutive Model for Strain-Controlled Strength Degradation of Rockmasses (SDR)

A. Kalos[1] · M. Kavvadas[1]

© Springer-Verlag GmbH Austria 2017

Abstract The paper describes a continuum, rate-independent, incremental plasticity constitutive model applicable in weak rocks and heavily fractured rockmasses, where mechanical behaviour is controlled by rockmass strength rather than structural features (discontinuities). The model describes rockmass structure by a generalised Hoek–Brown Structure Envelope (SE) in the stress space. Stress paths inside the SE are nonlinear and irreversible to better simulate behaviour at strains up to peak strength and under stress reversals. Stress paths on the SE have user-controlled volume dilatancy (gradually reducing to zero at large shear strains) and can model post-peak strain softening of brittle rockmasses via a structure degradation (damage) mechanism triggered by accumulated plastic shear strains. As the SE may strain harden with plastic strains, ductile behaviour can also be modelled. The model was implemented in the Finite Element Code Simulia ABAQUS and was applied in plane strain (2D) excavation of a cylindrical cavity (tunnel) to predict convergence-confinement curves. It is shown that small-strain nonlinearity, variable volume dilatancy and post-peak hardening/softening strongly affect the predicted curves, resulting in corresponding differences of lining pressures in real tunnel excavations.

Keywords Rockmass · Constitutive model · Plasticity · Nonlinear stiffness · Volume dilatancy · Structure degradation

✉ A. Kalos
alkalos83@gmail.com

1   Geotechnical Department, School of Civil Engineering, National Technical University of Athens (NTUA), 9, Iroon Polytechniou Street, 157 80 Zografou, Greece

List of symbols

SDR	Constitutive model for Strength Degradation of Rockmasses
SE	Structure Envelope
SPR	Stress Path Reversal
SSR	Stress Sign Reversal
a, σ_c, m_b, s	Genearlised Hoek–Brown parameters
$\boldsymbol{b}$	Rotation of the SE axis o with respect to the isotropic (σ) axis
$\mathbf{C}^e$	Tangent non-plastic stiffness matrix
c	Primary strength anisotropy parameter varied along each of the five shearing directions (values c_1, c_2, … c_5 along deviatoric axes S_1, S_2, … S_5)
d	State variable controlling the tensile strength of the rockmass, $d = (s/m_b)\,\sigma_c$
d_{in}, d_{fin}	Initial and final values of structure variable d
H	Plastic hardening modulus
$\mathbf{I}$	Unit isotopic tensor
K, G	Nonlinear bulk and shear moduli
$m_{b,\text{in}}$, $m_{b,\text{fin}}$	Initial and final values of structure variable m_b
n	Material constant controlling the non-plastic stiffness mean stress dependency
$\boldsymbol{P}$	Plastic potential tensor
P, $\boldsymbol{P}'$	Volumetric plastic potential and plastic potential deviator
p_{atm}	Atmospheric pressure ($p_{\text{atm}} \cong 101.3\ kPa$)
$\boldsymbol{Q}$	Gradient of the SE
Q, $\boldsymbol{Q}'$	Isotropic and deviatoric components of gradient $\boldsymbol{Q}$
q	Scalar stress deviator (shear stress)
r	Radial distance along the springline measuring from the tunnel centre ($r \geq R$, where R is the tunnel diameter)

$\boldsymbol{s}$	Stress deviator
u_R	Wall tunnel convergence
u_r	Radial convergence along the springline
$\dot{W}$	Second-order total work
$\dot{W}^p$	Second-order plastic work
γ	Material constant controlling the rate of stiffness reduction
$\dot{\boldsymbol{\varepsilon}}$	Strain increment
$\dot{\varepsilon}$, $\dot{\boldsymbol{e}}$	Volumetric strain and strain deviator increments
$\dot{\boldsymbol{\varepsilon}}^e$	Non-plastic strain increment
$\dot{\varepsilon}^e$, $\dot{\boldsymbol{e}}^e$	Non-plastic volumetric strain and strain deviator increments
$\dot{\boldsymbol{\varepsilon}}^p$	Plastic strain increment
$\dot{\varepsilon}^p$, $\dot{\boldsymbol{e}}^p$	Plastic volumetric strain and strain deviator increments
ε_a	Axial strain
ε_q^p	Scalar deviatoric plastic strain
$\dot{\varepsilon}_q^p$	Scalar deviatoric plastic strain increment
ε_{q,f_1}^p	Material constant equal to the accumulated plastic shear strain when variable m_b reaches the final value ($m_{b,fin}$)
ε_{q,f_2}^p	Material constant equal to the accumulated plastic shear strain when variable d reaches the final value (d_{fin})
ε_{vol}	Volumetric strain
ζ, n_q^p	Material constants controlling plastic volume dilatancy
θ_{in}, θ_{fin}	Initial and final values of variable θ
$\dot{\Lambda}$	Scalar plastic multiplier
v	Poisson's ratio
ξ, θ	State variables controlling the volumetric and deviatoric stiffness nonlinearity and irreversibility along non-plastic paths
ξ_{in}, ξ_{fin}	Initial and final values of variable ξ
ξ_0, θ_0	Values of variable ξ and θ at the SE axis
ξ_{SSR}, θ_{SSR}	Values of variable ξ and θ at SSR
$\boldsymbol{\sigma}$	Stress tensor
σ, p	Mean stress
$\dot{\boldsymbol{\sigma}}$	Stress increment
$\dot{\sigma}$, $\dot{\boldsymbol{s}}$	Mean stress and stress deviator increments
σ_1, σ_2, σ_3	Major, intermediate and minor principal stresses
$\boldsymbol{\sigma}_{rev}$	Stress at SPR
$\boldsymbol{\sigma}_{SSR}$	Stress at SSR

1 Introduction

The engineering behaviour of strong rockmasses with relatively sparse discontinuities (much weaker than the intermediate rock blocks) can be best described by constitutive models based on discrete mechanics. However, continuum mechanics models can be used in the analysis of a wide variety of practical rock engineering problems involving fractured rockmasses (with spacing of discontinuities much smaller than the characteristic dimension of the problem) and weak rocks (with strength of discontinuities comparable to the strength of the intermediate rock blocks).

The Hoek–Brown (HB) failure criterion, originally developed by Hoek and Brown (1980) and improved subsequently (Hoek 1983; Hoek et al. 1992, 1995; Hoek and Brown 1997), forms a sound basis for continuum modelling of rockmasses as it has a pressure-dependent curved failure envelope. Classical plasticity models using the HB failure criterion as yield surface (e.g. Mogi 1971; Pan and Hudson 1988; Wang and Kemeny 1995; Chang and Haimson 2000; Al-Ajmi and Zimmerman 2005; Priest 2005) predict a very large linear elastic domain (up to the peak strength), perfectly plastic strength (no hardening or softening) and nonzero dilatancy at large strains. On the contrary, real rockmasses are known to behave nonlinearly well before peak strength, are strongly strain softening (stress reduction in the post-peak domain) especially at low confinement, strongly dilate at small strains but eventually reach practically zero dilatancy (constant volume) at large shear strains. Several researchers have pointed out the need to use a non-associated flow rule to better control volume dilatancy, especially at large shear strains (e.g. Detournay 1986; Medhurst and Brown 1998; Yuan and Harrison 2004; Alejano and Alonso 2005) and the important effects of gradually reducing volume dilatancy in the design of tunnel linings (Kudoh et al. 1999; Alejano et al. 1999).

Modelling these features requires non-linear and often non-conservative "elasticity" inside the yield surface, non-associated flow rules which result in non-positive-definite stiffness and introduction of strain softening which can render the mathematical problem ill-posed, often leading to strain localisation/bifurcation (e.g. Frantziskonis and Desai 1988; Wang et al. 2007, 2011). Despite these potential mathematical problems, modelling the above features can be very useful in obtaining more realistic engineering solutions of complex rock engineering problems, especially in fractured and weak rockmasses.

The present paper describes and evaluates a continuum mechanics, incremental plasticity, rate-independent constitutive model for structure and strength degradation of rockmasses (SDR) due to accumulated plastic shear strains. The paper uses the term "structure" in the soil-mechanic sense which includes all strength and stiffness characteristics controlled by accumulated plastic shear strains, and the term "structure degradation" to describe strain softening and stiffness reduction in the post-peak domain where large plastic shear strains occur. As the model is rate

independent, "structure degradation" does not include time-dependent (creep) strength and stiffness degradation. The SDR model describes structure by a generalised Hoek–Brown Structure Envelope (SE) in the stress space. Unlike classical models, stress paths inside the SE are nonlinear and irreversible to better simulate nonlinear behaviour at strains up to the peak strength and under stress reversals (cyclic loading). For stress paths on the SE, the model uses a non-associated flow rule (for better control of dilatancy, especially at large shear strains where zero dilatancy is reached) and a structure degradation mechanism to predict post-peak strain softening (for brittle rockmasses) or strain hardening (for ductile rockmasses).

The SDR model is described via effective stresses, to include cases (mainly in weak low-permeability rocks) where excess pore water pressures can develop during loading, causing hydromechanical coupling (consolidation). As all stresses in the following are effective, the "prime" symbol (usually denoting effective stress) and the term "effective" are dropped to simplify formulae and text. Bold-face symbols indicate tensorial quantities, like the stress tensor ($\boldsymbol{\sigma}$) and the stress deviator ($\boldsymbol{s}$) which is defined as: $\boldsymbol{s} = \boldsymbol{\sigma} - \sigma\, \mathbf{I}$, where $\sigma \equiv p = \tfrac{1}{3}\,\boldsymbol{\sigma} : \mathbf{I}$ is the mean stress and ($\mathbf{I}$) is the unit isotropic tensor. The symbol ":" denotes the scalar product of two tensorial quantities. Finally, as the model is rate-independent, a "dot" over a symbol indicates an infinitesimal increment rather than true time rate of the corresponding quantity.

2 Stress Paths and Structure Envelope

In plasticity, material states are defined by a set of state variables; changes of material state are associated with changes of at least one state variable. In inviscid constitutive models (like the SDR), changes of material state are always associated with stress changes, while in viscous models material states may change even without stress changes (e.g. relaxation). State variables other than stress and strain (e.g. the accumulated plastic shear strain) are called "structure variables" and describe structure. Stress paths are the graphical representation of stress changes. Stress paths associated with changes of structure are called "plastic" paths; all other stress paths are called "non-plastic" paths and do not cause changes of structure. The present generalisation of classical "elastic" paths to "non-plastic" paths is required, because the SDR model includes inelastic (but non-plastic) strains even inside its "yield surface".

The SDR model describes material structure by a Structure Envelope (SE) in the stress space, analogous to the classical "yield surface". The term "yield" has been replaced by "structure" because "yield" implies the onset

of nonlinearity, while the present model includes nonlinear response even inside the SE. Stress paths inside the SE are non-plastic (i.e. nonlinear but causing no change of structure), while stress paths on the SE are plastic (causing changes of structure). Paths outside the SE are not possible, as any stress path tending to move outside the SE, pulls the SE with it causing a plastic path. A stress point on the SE may tend to move towards the interior of the SE either by pulling the SE with it causing a plastic path or by retreating from the SE causing a non-plastic path. The behaviour of the SDR model inside the SE is nonlinear and associated with irreversible (inelastic) strains; thus, non-plastic paths of the SDR model are not equivalent to "elastic" paths of plasticity models with classical yield surfaces.

The Structure Envelope SE of the SDR model is a Hoek–Brown (HB) curved open surface in a stress hyperspace consisting of the isotropic axis $\sigma = (\sigma_x + \sigma_y + \sigma_z)/3$ and a five-dimensional deviatoric hyperplane $\boldsymbol{s}$ (Fig. 1):

$$
\begin{aligned}
F(\boldsymbol{\sigma}&, m_b, d) \\
&\equiv \left\{ \frac{3}{2}\,\frac{1}{\sigma_c^2}\,\frac{1}{c^2}\,[\boldsymbol{s} - (\sigma + d)\,\boldsymbol{b}] : [\boldsymbol{s} - (\sigma + d)\,\boldsymbol{b}] \right\}^{\frac{1}{2a}} \\
&\quad - \frac{m_b}{\sigma_c} \left\{ (\sigma + d) - \frac{1}{3}\,\sqrt{\frac{3}{2}\,\frac{1}{c^2}\,[\boldsymbol{s} - (\sigma + d)\,\boldsymbol{b}] : [\boldsymbol{s} - (\sigma + d)\,\boldsymbol{b}]} \right\} \\
&= 0
\end{aligned}
$$

(1)

The model is described in a six-dimensional space (isotropic plus five deviatoric components), rather than the usual two-dimensional space (isotropic plus one compound shear) because most rock engineering problems are two or three dimensional and thus involve more than two stress and strain components. The five independent deviatoric
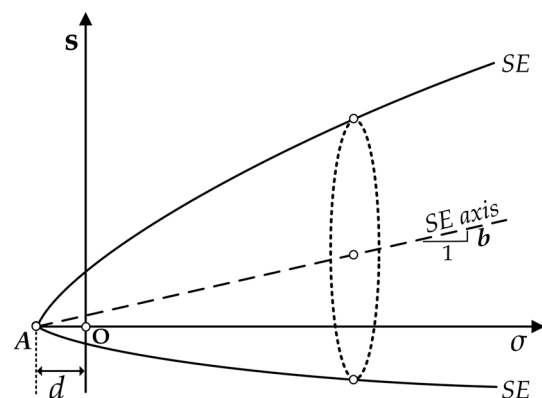

Fig. 1 Structure Envelope (SE) of the SDR model represented by a curved open surface in the stress space. The large domain inside the SE includes nonlinear stress paths associated with irreversible but non-plastic strains. The horizontal axis plots the isotropic stress (σ), while the vertical axis plots all five deviatoric stresses in a deviatoric hyperplane, depicted in the figure as a single axis ($\boldsymbol{s}$)

components include the following deviatoric stresses (Kavvadas and Amorosi 2000) $S_1 = \left(2\sigma_y - \sigma_x - \sigma_z\right)$ $/\sqrt{6}$, $S_2 = (\sigma_z - \sigma_x)/\sqrt{2}$, $S_3 = \sqrt{2}\,\sigma_{xy}$, $S_4 = \sqrt{2}\,\sigma_{xz}$, $S_5 = \sqrt{2}\,\sigma_{yz}$ and the corresponding energy conjugate deviatoric strains $E_1 = \left(2\varepsilon_y - \varepsilon_x - \varepsilon_z\right)/\sqrt{6}$, $E_2 = (\varepsilon_z - \varepsilon_x)/\sqrt{2}$, $E_3 = \sqrt{2}\,\varepsilon_{xy}$, $E_4 = \sqrt{2}\,\varepsilon_{xz}$, $E_5 = \sqrt{2}\,\varepsilon_{yz}$ plus the isotropic stress $\sigma = \left(\sigma_x + \sigma_y + \sigma_z\right)/3$ and corresponding volumetric strain $\varepsilon = \left(\varepsilon_x + \varepsilon_y + \varepsilon_z\right)$. In simpler configurations fewer components are involved; for example, uniaxial compression or triaxial loading along axis "y" activates only stresses (σ, S_1) and strains (ε, E_1), while plane strain in the xy-plane activates only stresses (σ, S_1, S_2) and strains (ε, E_1, E_2).

The SE axis (line: $\boldsymbol{s} = (\sigma + d)\,\boldsymbol{b}$) is rotated with respect to the isotropic axis by a vector ($\boldsymbol{b}$) to allow better control of compressive and tensile strengths. Cross sections of the SE normal to the isotropic axis (i.e. on the deviatoric π-plane) are circles with centre on the SE axis and radius (for $a = 0.5$):

$$R = \frac{\sqrt{6}}{18}\,c\,(\sigma_c\,m_b)\left[\sqrt{1 + 36\,\frac{(\sigma + d)}{\sigma_c\,m_b}} - 1\right] \qquad (2)$$

To further increase flexibility, material constant (c) can vary along each of the five shearing directions (values c_1, c_2, ... c_5 along deviatoric axes S_1, S_2, ... S_5 respectively) allowing for shear strength anisotropy, i.e. different strengths, equal to $c_1\,\sigma_c$, $c_2\,\sigma_c$, ..., $c_5\,\sigma_c$, along each of the five shearing directions (Kavvadas and Amorosi 2000). Obviously, the model can be simplified by eliminating several of its parameters (e.g. $\boldsymbol{b} = 0$ and $c_1 = c_2 = \cdots = c_5$) at the cost of eliminating the corresponding features.

The SE includes four material constants (a, σ_c, c, $\boldsymbol{b}$) and two structure variables (m_b, d) which are analogous to the four material constants (a, σ_c, m_b, s) of the generalised Hoek–Brown failure criterion:

- a: parameter of the generalised HB failure criterion (equal to 0.50 in the HB failure criterion).
- σ_c: uniaxial compressive strength (UCS) of the intact rock (HB failure criterion).
- c: parameter related to strength anisotropy when varied along each shearing direction.
- $\boldsymbol{b}$: rotation of the axis of the SE with respect to the isotropic (σ) axis. Controls strength differences during loading along the positive and negative direction of each deviatoric stress axis (e.g. along S_1 and $-S_1$) in a way similar to, but simpler than, the Lode angle (third stress invariant). For $\boldsymbol{b} = 0$, the SE is oriented along the isotropic axis (HB failure criterion).
- m_b: state variable controlling the opening of the SE, in a way similar to an "equivalent" friction angle of the

rockmass. It is used to control post-peak strain softening or hardening. In brittle rockmasses, m_b degrades with accumulated plastic strains to model the gradual transition from peak to residual (lower) friction angle and the resulting strain softening. In ductile rockmasses, m_b increases continuously with accumulated plastic strains to model strain hardening. In the classical HB failure criterion, m_b is a material constant.

- d: state variable controlling the tensile strength of the rockmass. Degrades with plastic strains to model the gradual reduction of tensile strength at large deformations. In the HB failure criterion, (d) is a material constant related to the HB constant (s) by the formula: $d = (s/m_b)\,\sigma_c$.

The SE envelope of the SDR model (Eq. 1) reduces to the generalised Hoek–Brown failure criterion (Hoek and Brown 1997):

$$\sigma_1 = \sigma_3 + \sigma_c \left(\frac{m_b}{\sigma_c}\,\sigma_3 + s\right)^a \qquad (3)$$

in triaxial stress conditions ($\sigma_2 = \sigma_3$, where σ_1 and σ_3 are the major and minor principal stresses, respectively), if $c = 1$, $\boldsymbol{b} = 0$ and $d = (s/m_b)\,\sigma_c$.

3 Behaviour Inside the Structure Envelope

Along paths inside the SE (non-plastic paths), an infinitesimal stress increment ($\dot{\boldsymbol{\sigma}}$) causes only non-plastic strain increments ($\dot{\boldsymbol{\varepsilon}}^e$) calculated by the formula:

$$\dot{\boldsymbol{\sigma}} = \mathbf{C}^e : \dot{\boldsymbol{\varepsilon}}^e \qquad (4)$$

where ($\mathbf{C}^e$) is the tangent non-plastic stiffness. For the common case of isotropic tangent stiffness, Eq. (4) can be decomposed in volumetric and deviatoric parts including the corresponding stress ($\dot{\sigma}$, $\dot{\boldsymbol{s}}$) and strain ($\dot{\varepsilon}^e$, $\dot{\boldsymbol{e}}^e$) components:

$$\dot{\sigma} = K\,\dot{\varepsilon}^e \quad \text{and} \quad \dot{\boldsymbol{s}} = 2G\,\dot{\boldsymbol{e}}^e \qquad (5)$$

where (K) and (G) are non-linear bulk and shear moduli, respectively, calculated by the formulae:

$$K = \xi\,p_{\text{atm}}\left(\frac{\sigma + d}{p_{\text{atm}}}\right)^n \quad \text{and} \quad G = \theta\,K. \qquad (6)$$

Exponent n is a material constant, p_{atm} is the atmospheric pressure ($p_{\text{atm}} \cong 101.3$ kPa) used for dimensional consistency, and $\theta = G/K = {}^3\!/_2\,(1 - 2v)/(1 + v)$, where "$v$" is a variable Poisson's ratio. The (K) and (G) moduli are not only pressure dependent, but they also depend on the shear stresses via (ξ, θ) making behaviour inside the SE non-linear and irreversible.

Variables (ξ, θ) control volumetric and deviatoric stiffness non-linearity and irreversibility via the location of the stress (σ) inside the SE, measured by the value $F(\sigma)$ of the SE function and the direction of the stress path. When a stress point inside the SE moves towards the SE, the F function increases (reaching $F = 0$ when the point reaches the SE), while F decreases when the stress point moves away from the SE towards its axis (where F reaches a minimum value). A stress path reversal (SPR) occurs when a stress path changes direction by more than 90° (the dot product of the old and new directions is negative). SPRs are associated either with change from loading to unloading (when the F value changes from increasing to decreasing) or with change from unloading to loading (when the F value changes from decreasing to increasing). A stress sign reversal (SSR) occurs when a stress path changes direction by less than 90° (the dot product of the old and new directions is positive) and the F value changes from decreasing to increasing (i.e. the stress path changes from unloading to loading). This case corresponds to the passage of a stress path from the SE axis or close to the SE axis without appreciable change in direction; in simple cases it corresponds to full unloading to zero shear stress and then loading in the opposite shear stress direction.

At initial conditions and after a SPR from stress σ_{rev}, stiffness is reset to high (initial) values $(\xi_{\text{in}}, \theta_{\text{in}})$ corresponding to the very small-strain stiffness of the material. Typically, ξ_{in} is calculated by methods like those described by Hoek et al. (2002) and Hoek and Diederichs (2006) and $\theta_{\text{in}} = 0.60$ (corresponding to initial Poisson ratio $v_{\text{in}} = 0.25$). For monotonic stress paths inside the SE, the stiffness gradually reduces towards low (final) values $(\xi_{\text{fin}}, \theta_{\text{fin}})$ reached at the SE. For typical cases (e.g. Mas Ivars et al. 2011; Ma et al. 2013), $\xi_{\text{fin}} = 0.20 \, \xi_{\text{in}}$ (corresponding to large strain stiffness equal to 20% of the initial value) and $\theta_{\text{fin}} = 0.21$ (corresponding to large strain Poisson ratio $v_{\text{fin}} = 0.40$).

Variables (ξ, θ) are calculated by the following formulae:

- *Initial stress path and stress paths after a SPR from Unloading to Loading:*

$$\xi = \xi_{\text{fin}} \left\{ 1 + \frac{F(\sigma)}{F(\sigma_{\text{rev}})} \left[\left(\frac{\xi_{\text{fin}}}{\xi_{\text{in}}} \right)^{\frac{1}{\gamma}} - 1 \right] \right\}^{-\gamma} \quad (7a)$$

$$\theta = \theta_{\text{fin}} \left\{ 1 + \frac{F(\sigma)}{F(\sigma_{\text{rev}})} \left[\left[\frac{\theta_{\text{fin}}}{\theta_{\text{in}}} \right]^{\frac{1}{\gamma}} - 1 \right] \right\}^{-\gamma} \quad (7b)$$

where (γ) is a material constant controlling the rate of stiffness reduction. These formulae gradually reduce (ξ, θ) from the (high) initial values $(\xi_{\text{in}}, \theta_{\text{in}})$ at the point of stress reversal to the (low) final values $(\xi_{\text{fin}}, \theta_{\text{fin}})$ when the SE is reached (where F becomes zero).

- *Stress paths after a SPR from Loading to Unloading:*

$$\xi = \xi_0 + (\xi_{\text{in}} - \xi_0) \, \frac{F(\sigma) - F(\sigma, \, s = (\sigma + d)\, b)}{F(\sigma_{\text{rev}}) - F(\sigma, \, s = (\sigma + d)\, b)} \quad (8a)$$

$$\theta = \theta_0 + (\theta_{\text{in}} - \theta_0) \, \frac{F(\sigma) - F(\sigma, \, s = (\sigma + d)\, b)}{F(\sigma_{\text{rev}}) - F(\sigma, \, s = (\sigma + d)\, b)}. \quad (8b)$$

These formulae gradually reduce (ξ, θ) from the (high) initial values $(\xi_{\text{in}}, \theta_{\text{in}})$ at the point of stress reversal to the user-defined values (ξ_0, θ_0) at the SE axis (where $s = (\sigma + d)\, b$). If the stress path does not cross the SE axis, stress sign reversal (SSR) will occur at the point closest to the SE axis, where (ξ, θ) will reach some values $(\xi_{\text{SSR}}, \theta_{\text{SSR}})$ larger than (ξ_0, θ_0). Typically (ξ_0, θ_0) are equal to about 80% of the corresponding initial values.

- *Loading after a SSR at point (σ_{SSR}):*

$$\xi = \xi_{\text{fin}} \left\{ 1 + \frac{F(\sigma)}{F(\sigma_{\text{SSR}})} \left[\left(\frac{\xi_{\text{fin}}}{\xi_{\text{SSR}}} \right)^{\frac{1}{\gamma}} - 1 \right] \right\}^{-\gamma} \quad (9a)$$

$$\theta = \theta_{\text{fin}} \left\{ 1 + \frac{F(\sigma)}{F(\sigma_{\text{SSR}})} \left[\left[\frac{\theta_{\text{fin}}}{\theta_{\text{SSR}}} \right]^{\frac{1}{\gamma}} - 1 \right] \right\}^{-\gamma}. \quad (9b)$$

These formulae gradually reduce (ξ, θ) from the values reached at the point of SSR $(\xi_{\text{SSR}}, \theta_{\text{SSR}})$ to the final values $(\xi_{\text{fin}}, \theta_{\text{fin}})$ as the stress point approaches the SE (same rule as Eqs. 7 above).

Figure 2 illustrates the application of the above formulae to predict non-linear (NL) stress paths inside the SE by comparing them with the corresponding "linear" (L) behaviour (ξ, θ are constant and equal to their initial values $\xi_{\text{fin}}, \theta_{\text{fin}}$) during a drained cyclic triaxial stress path starting from an isotropic state (point A). As the "linear" path is also pressure dependent, the "linear" path is slightly curved because the mean stress varies slightly in triaxial loading. The sample is sheared in the non-plastic domain (inside the SE) until point B (slightly below the SE) and then is subjected to loading and unloading cycles: A–B–C–D (without reaching stress sign reversal) and then D–E–F–G–H (reaching twice stress sign reversal at points E and G) with the final point H reaching the SE. At points of stress path reversal (B, C, D, F), the variables (θ, ξ) are reset to the initial (high) values. Unloading path D-E-F and subsequent loading path F-G-H include two points of stress sign reversal (E and G). The effects of nonlinearity are very significant and permit the prediction of significant hysteretic damping during cyclic loading.
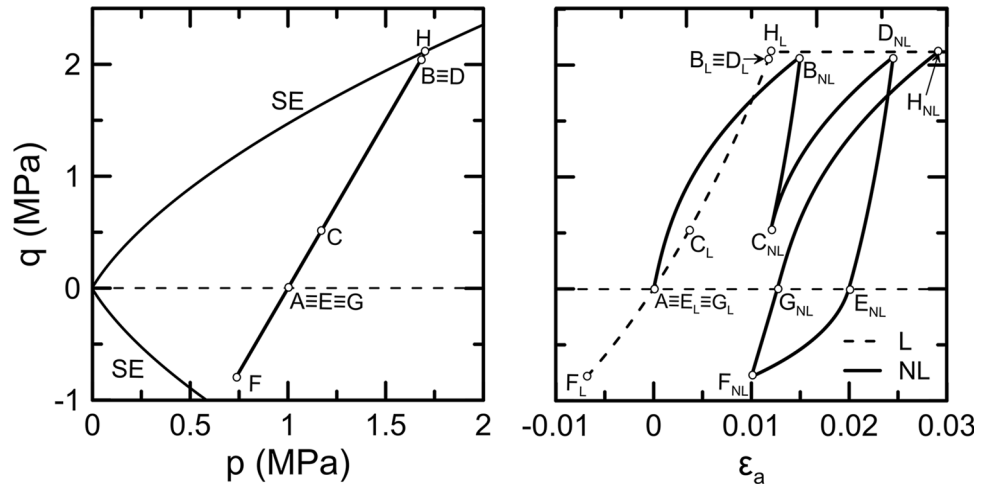
4 Hardening Rules

Plastic paths, i.e. stress paths on the Structure Envelope (SE), cause strain increments ($\dot{\varepsilon}$) including components in addition to those occurring during non-plastic paths, called plastic strain increments $\dot{\boldsymbol{\varepsilon}}^p$):

$$\dot{\boldsymbol{\varepsilon}}^p = \dot{\boldsymbol{\varepsilon}} - \dot{\boldsymbol{\varepsilon}}^e \qquad (10a)$$

Equation (10a) can be decomposed in volumetric and deviatoric (shear) parts:

$$\dot{\varepsilon}^p = \dot{\varepsilon} - \dot{\varepsilon}^e, \qquad \dot{\boldsymbol{e}}^p = \dot{\boldsymbol{e}} - \dot{\boldsymbol{e}}^e \qquad (10b)$$

As changes of material structure (expressed by the evolution of the SE) occur only in plastic paths, they must depend on the plastic strain increments only. In plasticity, changes of material structure are expressed via the hardening rules. The SDR model includes hardening rules to control the evolution of structure variables (m_b, d) with plastic strain increments.

4.1 Hardening of the SE "Friction Angle" (variable m_b)

The Generalised Hoek–Brown model assumes that strength parameter (m_b), which controls the opening of the SE (i.e. an equivalent "friction angle"), is a material constant and thus the classical HB model predicts elastic–perfectly plastic response, i.e. shear stress remains constant when the failure criterion is reached. Real rockmasses, however, have either ductile response (strain harden, i.e. shear stress increases after yielding) or brittle response (strain soften, i.e. shear stress decreases after peak strength) at large strains (e.g. Crouch 1970; Gerogiannopoulos and Brown 1978).

The SDR model uses the following hardening rule to model strain hardening and strain softening by the gradual

evolution of structure variable (m_b) between the initial and final values ($m_{b,in}$, $m_{b,fin}$) with plastic shear strains:

$$\dot{m}_b = -2\left(m_{b,in} - m_{b,fin}\right)\left(\frac{\varepsilon_q^p}{\varepsilon_{q,f_1}^p}\right)\left(1 - \frac{\varepsilon_q^p}{\varepsilon_{q,f_1}^p}\right)\dot{\varepsilon}_q^p \text{ for } 0 \le \varepsilon_q^p \le \varepsilon_{q,f_1}^p$$

$$(11a)$$

$$\dot{m}_b = 0 \quad \text{for} \quad \varepsilon_q^p > \varepsilon_{q,f_1}^p \qquad (11b)$$

where $\dot{\varepsilon}_q^p = \sqrt{2/3(\dot{\boldsymbol{e}}^p : \dot{\boldsymbol{e}}^p)}$ is the scalar modulus of the plastic shear strain increment and $\varepsilon_q^p = \sum \dot{\varepsilon}_q^p$ is the accumulated plastic shear strain. Response is strain hardening if $m_{b,fin} > m_{b,in}$ and strain softening in the opposite case. Parameter ε_{q,f_1}^p is a material constant equal to the accumulated plastic shear strain when variable m_b reaches the final value ($m_{b,fin}$). Larger values of ε_{q,f_1}^p give slower m_b evolution rates and thus slower transition to the residual strength ($m_{b,fin}$). The SDR model can independently control the magnitude of strain softening/hardening (by $m_{b,in}$ and $m_{b,fin}$) and the rate of strength degradation (by ε_{q,f_1}^p).

Figure 3 shows the effect of structure variable (m_b) on the shape of the shear stress (q)–axial strain (ε_a) curve during a drained triaxial test (path A–B–C) starting from an isotropic state A ($\sigma = 1$ MPa), for three m_b values: $m_{b,fin} = m_{b,in}$ (perfectly plastic), $m_{b,fin} = 2\ m_{b,in}$ (hardening) and $m_{b,fin} = 0.5\ m_{b,in}$ (softening). For simplicity, pre-peak response is assumed to be linear.

4.2 Hardening of SE "Cohesion" (variable d)

The generalised Hoek–Brown model assumes that cohesion parameter (d), which controls the position of the SE apex on the isotropic axis (Fig. 1), is a constant related to the classical HB constant (s) by the formula: $d = (s/m_b)\ \sigma_c$. The SDR model assumes that (d) is a structure variable which evolves with plastic shear strains between initial and

Fig. 3 Effect of structure variable (m_b) on the shape of the shear stress (q)–axial strain (ε_a) curve
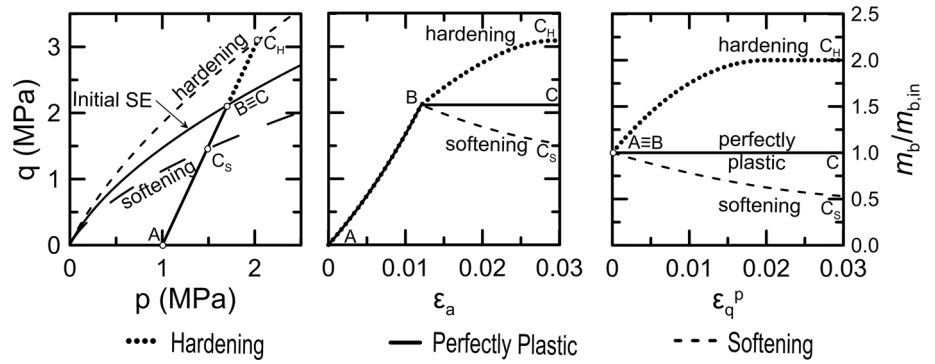
final values (d_{in}, d_{fin}), according to the following hardening rule:

$$\dot{d} = -2(d_{in} - d_{fin}) \left(\frac{\varepsilon_q^p}{\varepsilon_{q,f2}^p}\right) \left(1 - \frac{\varepsilon_q^p}{\varepsilon_{q,f2}^p}\right) \dot{\varepsilon}_q^p \quad \text{for} \quad 0 \le \varepsilon_q^p \le \varepsilon_{q,f2}^p$$

(12a)

$$\dot{d} = 0 \quad \text{for} \quad \varepsilon_q^p > \varepsilon_{q,f2}^p$$

(12b)

usually $d_{fin} = 0$ (cohesion is fully eliminated at large shear strains). Parameter $\varepsilon_{q,f2}^p$ is a material constant equal to the accumulated plastic shear strain when variable d reaches the final value (d_{fin}). Larger values of $\varepsilon_{q,f2}^p$ give slower d evolution rates and thus slower transition to the residual cohesion.

Figure 4 shows the effect of the accumulated plastic shear strain ($\varepsilon_{q,f2}^p$) on the softening branch of the shear stress (q)–axial strain (ε_a) curve during a drained triaxial test (path A-B-C) starting from an isotropic state A ($\sigma = 1$ MPa), for three values of $\varepsilon_{q,f2}^p$: 0.04, 0.06 and 0.08. In all cases: $d_{fin} = 0.5\, d_{in}$ and $m_{b,fin} = 0.5\, m_{b,in}$. For simplicity, pre-peak response is assumed to be linear.

5 Flow Rule and Plastic Modulus

In incremental plasticity, the flow rule gives the plastic strain increment ($\dot{\varepsilon}^p$) along plastic paths (on the SE) by the formula:

$$\dot{\boldsymbol{\varepsilon}}^p = \dot{\Lambda}\, \boldsymbol{P}$$

(13a)

or equivalently (for strains expressed via volumetric and deviatoric components):

$$\dot{\varepsilon}^p = \dot{\Lambda}\, P \qquad \dot{\boldsymbol{e}}^p = \dot{\Lambda}\, \boldsymbol{P}'$$

(13b)

In the above formulae, the scalar plastic multiplier $\dot{\Lambda}$ controls the magnitude of the plastic strain increment, while the plastic potential tensor $\boldsymbol{P}$ (having isotropic and deviatoric components P and $\boldsymbol{P}'$, respectively) gives its direction.
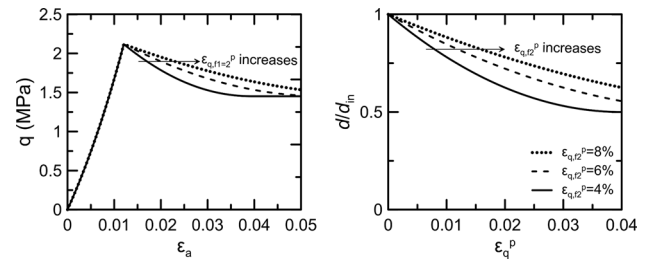

Fig. 4 Effect of the accumulated plastic shear strain ($\varepsilon_{q,f2}^p$) on the softening branch of the shear stress (q)–axial strain (ε_a) curve

Flow rules are "associated" if the plastic potential $\boldsymbol{P}$ is equal to the gradient $\boldsymbol{Q} = \partial F/\partial \boldsymbol{\sigma}$ of the Structure Envelope (SE, Eq. 1), which has the following isotropic (Q) and deviatoric ($\boldsymbol{Q}'$) components:

$$Q = \boldsymbol{Q} : \mathbf{I} = -\left\{\frac{1}{2}\frac{1}{c^2}\left[\boldsymbol{s} - (\sigma+d)\,\boldsymbol{b}\right] : \right.$$
$$\boldsymbol{b}\left\{\frac{3}{a}\frac{1}{\sigma_c^2}\left\{\frac{3}{2}\frac{1}{\sigma_c^2}\frac{1}{c^2}\left[\boldsymbol{s} - (\sigma+d)\,\boldsymbol{b}\right] : \left[\boldsymbol{s} - (\sigma+d)\,\boldsymbol{b}\right]\right\}^{\frac{1}{2a}-1}\right.$$
$$\left.+\frac{m_b}{\sigma_c}\left\{\frac{3}{2}\frac{1}{\sigma_c^2}\frac{1}{c^2}\left[\boldsymbol{s} - (\sigma+d)\,\boldsymbol{b}\right] : \left[\boldsymbol{s} - (\sigma+d)\,\boldsymbol{b}\right]\right\}^{-\frac{1}{2}}\right\} + \frac{m_b}{\sigma_c}\right\}$$

(14a)

$$\boldsymbol{Q}' = \boldsymbol{Q} - \frac{1}{3}Q\,\mathbf{I} = \frac{1}{2}\frac{1}{c^2}\left[\boldsymbol{s} - (\sigma+d)\,\boldsymbol{b}\right]$$
$$\left\{\frac{3}{a}\frac{1}{\sigma_c^2}\left\{\frac{3}{2}\frac{1}{\sigma_c^2}\frac{1}{c^2}\left[\boldsymbol{s} - (\sigma+d)\,\boldsymbol{b}\right] : \left[\boldsymbol{s} - (\sigma+d)\,\boldsymbol{b}\right]\right\}^{\frac{1}{2a}-1}\right.$$
$$\left.+\frac{m_b}{\sigma_c}\left\{\frac{3}{2}\frac{1}{\sigma_c^2}\frac{1}{c^2}\left[\boldsymbol{s} - (\sigma+d)\,\boldsymbol{b}\right] : \left[\boldsymbol{s} - (\sigma+d)\,\boldsymbol{b}\right]\right\}^{-\frac{1}{2}}\right\}$$

(14b)

Classical constitutive models based on the HB failure criterion use associated flow rules and thus predict non-zero dilatancy even at large strains, since $P = Q \neq 0$ (always) and thus Eq. (13b) gives $\dot{\varepsilon}^p \neq 0$. To better control volume dilatancy in the post-peak domain and achieve zero dilatancy at large accumulated shear strains, the SDR model uses a non-associated flow rule for the volumetric

component only. Thus, the volumetric (P) and deviatoric (P') components of the plastic potential tensor ($\boldsymbol{P}$) are:

$$P = \zeta\, Q\ \exp\left(-n_q^p\, \varepsilon_q^p\right) \quad \text{and} \quad \boldsymbol{P'} = \boldsymbol{Q'} \qquad (15)$$

where (ζ, n_q^p) are material constants controlling plastic volume dilatancy. Equation (15) ensures that the rockmass reaches a constant volume condition (zero dilatancy) at large plastic shear strains (ε_q^p), as $P \rightarrow 0$ for large (ε_q^p), and Eq. (13b) gives $\dot{\varepsilon}^p = 0$ for $P = 0$. Zero dilatancy at large strains is common in weak and heavily fractured rock-masses and has significant implications in the predicted ground pressure on tunnel linings; classical models (predicting nonzero dilatancy at large strains) artificially increase tunnel wall convergence, resulting in significantly larger tunnel lining pressures, especially in stiff linings, commonly used in weak rockmasses.

The plastic multiplier $\dot{\Lambda}$ is usually expressed via a scalar plastic modulus (H) defined by the formula:

$$\dot{\Lambda} = \frac{1}{H}\left(\boldsymbol{Q}\ :\ \dot{\boldsymbol{\sigma}}\right) = \frac{1}{H}\left(Q\,\dot{\sigma} + \boldsymbol{Q'}\ :\ \dot{\boldsymbol{s}}\right) \qquad (16)$$

which ensures continuity of plastic strain increments between plastic and non-plastic paths from a point on the SE, by requiring that stress paths tangent to the SE ($\dot{\boldsymbol{\sigma}}$ perpendicular to $\boldsymbol{Q}$) cause zero $\dot{\Lambda}$ and thus zero plastic strain increments (from Eqs. 13 and 16).

For plastic paths, the plastic modulus (H) is calculated by the consistency condition which exploits the requirement that the stress point remains on the SE:

$$dF(\boldsymbol{\sigma},\, m_b,\, d) = 0 \quad \Rightarrow$$
$$\frac{\partial F}{\partial \boldsymbol{\sigma}} : \dot{\boldsymbol{\sigma}} + \frac{\partial F}{\partial m_b} : \dot{m}_b + \frac{\partial F}{\partial d} : \dot{d} = 0 \qquad (17)$$

As $\boldsymbol{Q} = (\partial F / \partial \boldsymbol{\sigma})$, assuming that the increments of the hardening variables ($\dot{m}_b$, $\dot{d}$) are proportional to the plastic multiplier $\dot{\Lambda}$, i.e. $\dot{m}_b = \dot{\Lambda}\, h_m$ and $\dot{d} = \dot{\Lambda}\, h_d$, and substitution in Eq. (17) and use of Eq. (16) gives the scalar plastic modulus H:

$$H = -\left(\frac{\partial F}{\partial m_b}\, h_m + \frac{\partial F}{\partial d}\, h_d\right) \qquad (18)$$

where

$$\frac{\partial F}{\partial m_b} = -\frac{1}{\sigma_c}\left\{(\sigma + d) - \frac{1}{3}\sqrt{\frac{3}{2}\frac{1}{c^2}\,[\boldsymbol{s} - (\sigma + d)\,\boldsymbol{b}] : [\boldsymbol{s} - (\sigma + d)\,\boldsymbol{b}]}\right\}$$
$$\text{and}\ \ \frac{\partial F}{\partial d} = Q \qquad (19)$$

Finally, for a given strain increment ($\dot{\boldsymbol{\varepsilon}}$), the plastic multiplier $\dot{\Lambda}$ is calculated in terms of the scalar plastic modulus H using Eq. (16):

$$\dot{\Lambda} H = \boldsymbol{Q}\ :\ \dot{\boldsymbol{\sigma}} = \boldsymbol{Q} : (\mathbf{C}^e : \dot{\boldsymbol{\varepsilon}}^e) = \boldsymbol{Q} : \mathbf{C}^e : (\dot{\boldsymbol{\varepsilon}} - \dot{\boldsymbol{\varepsilon}}^p) = \boldsymbol{Q}$$
$$: \mathbf{C}^e : \dot{\boldsymbol{\varepsilon}} - \dot{\Lambda}\,(\boldsymbol{Q} : \mathbf{C}^e : \boldsymbol{P})$$
$$\Rightarrow$$
$$\dot{\Lambda} = \frac{\boldsymbol{Q}\ :\ \mathbf{C}^e\ :\ \dot{\boldsymbol{\varepsilon}}}{H\ +\ \boldsymbol{Q} : \mathbf{C}^e : \boldsymbol{P}} \qquad (20)$$

As the SDR model uses non-linear elasticity, non-associated flow rule and permits strain softening, stability and uniqueness of the numerical solution can be an issue. In incremental plasticity, stability and uniqueness are ensured by satisfaction of Hill's (1958) stability postulate, valid also for non-associated flow rules (Mroz 1963; Mandel 1966), which requires that the second-order work during an infinitesimal elastoplastic loading increment is positive: $\dot{W} = \dot{\boldsymbol{\sigma}} : \dot{\boldsymbol{\varepsilon}} > 0$

Stress paths inside the SE (non-plastic paths) always satisfy Hill's postulate because the non-plastic stiffness ($\mathbf{C}^e$) is positive definite and $\dot{W} = \dot{\boldsymbol{\sigma}} : \dot{\boldsymbol{\varepsilon}} = \dot{\boldsymbol{\sigma}} : \dot{\boldsymbol{\varepsilon}}^e = \dot{\boldsymbol{\varepsilon}}^e : \mathbf{C}^e : \dot{\boldsymbol{\varepsilon}}^e > 0$.

For plastic paths (on the SE), the SDR model ensures stability and uniqueness if $\dot{\Lambda} > 0$ for strain hardening and $\dot{\Lambda} < 0$ for strain softening. The proof is given below.

$\dot{W} = \dot{\boldsymbol{\sigma}} : \dot{\boldsymbol{\varepsilon}} > 0 \quad \Rightarrow \quad \dot{\boldsymbol{\sigma}} : \dot{\boldsymbol{\varepsilon}}^p > -\dot{\boldsymbol{\sigma}} : \dot{\boldsymbol{\varepsilon}}^e = -(\dot{\boldsymbol{\varepsilon}}^e : C^e) : \dot{\boldsymbol{\varepsilon}}^e = -(\dot{\boldsymbol{\varepsilon}}^e : C^e : \dot{\boldsymbol{\varepsilon}}^e) \leq 0$, since ($\mathbf{C}^e$) is positive definite. Based on the above, Hill's stability postulate is satisfied if:

$$\dot{\boldsymbol{\sigma}}\ :\ \dot{\boldsymbol{\varepsilon}}^p\ >\ 0\ \Rightarrow\ \dot{\boldsymbol{\sigma}}\ :\ \left(\dot{\Lambda}\,\mathbf{P}\right)\ >\ 0\ \Rightarrow\ \dot{\Lambda}\,\left(\dot{\boldsymbol{\sigma}}\ :\ \mathbf{P}\right)\ >\ 0$$

Based on the above, Hill's stability postulate is satisfied if $\dot{\Lambda} > 0$ during strain hardening ($\dot{\boldsymbol{\sigma}} : \boldsymbol{P} > 0$) and if $\dot{\Lambda} < 0$ during strain softening ($\dot{\boldsymbol{\sigma}} : \boldsymbol{P} < 0$). The numerator of Eq. (20) is always positive (plastic loading), and thus, the sign of $\dot{\Lambda}$ is the same as the sign of ($H + \boldsymbol{Q} : \mathbf{C}^e : \boldsymbol{P}$). Furthermore, $\boldsymbol{Q} : \mathbf{C}^e : \boldsymbol{P} > 0$ in all cases. Thus, for strain hardening paths ($H > 0$), always $\dot{\Lambda} > 0$ and thus stability and uniqueness are always ensured. For strain softening paths ($H < 0$), stability and uniqueness are ensured if ($H + \boldsymbol{Q} : \mathbf{C}^e : \boldsymbol{P}$) $< 0 \Rightarrow H < -(\boldsymbol{Q} : \mathbf{C}^e : \boldsymbol{P})$ but may not be ensured if $-(\boldsymbol{Q} : \mathbf{C}^e : \boldsymbol{P}) < H < 0$.

6 Summary of Model Parameters and State Variables

The model uses the following state variables. In numerical analyses, their values are set at the beginning of the calculation; subsequently, their values are updated automatically in each analysis step.

1. $\boldsymbol{\sigma}$: current effective stress
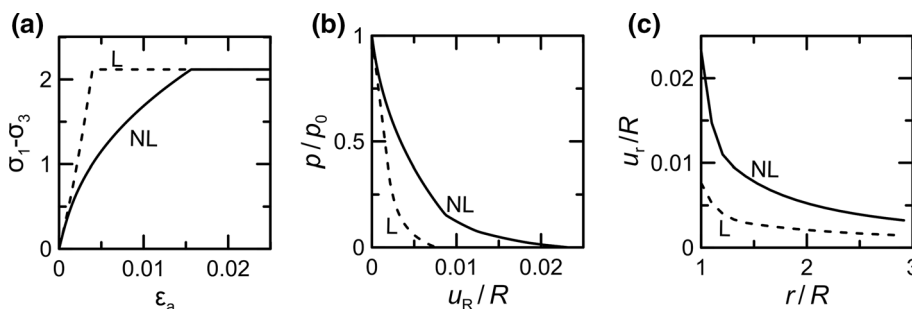2. m_b and d: structure variables. Define the size of the SE surface.

Fig. 5 Effect of stress–strain non-linearity (L—linear pressure-dependent elasticity; NL—nonlinear pressure-dependent elasticity) on the convergence (u_R)–confinement (p) curve of tunnel excavation: **a** Drained triaxial shear stress ($\sigma_1-\sigma_3$) versus axial strain (ε_a) curves used in the analyses. **b** convergence (u_R)–confinement (p) curves and **c** radial convergence (u_r) versus distance (r) from the tunnel axis at full tunnel excavation ($p = 0$)

3. $F(\boldsymbol{\sigma}_{rev})$: value of the SE function at the point of the last stress path reversal. At start, it is equal to $F(\boldsymbol{\sigma})$.
4. ε_q^p: accumulated plastic shear strain. At start it is set to zero.

In the most general application, the model uses the following twenty (20) material constants:

1. a, σ_c, c, $\boldsymbol{b}$: control the shape and orientation of the Structure Envelope.
2. (ξ_{in}, θ_{in}), $(\xi_{fin}, \theta_{fin})$, (ξ_0, θ_0), n, γ: control nonlinear behaviour along non-plastic paths (inside the SE).
3. $(m_{b,in}, m_{b,fin}, \varepsilon_{q,f1}^p)$, $(d_{in}, d_{fin}, \varepsilon_{q,f2}^p)$: control the evolution of structure variables m_b, d.
4. ζ, n_q^p: control volume dilatancy along plastic paths. The flow rule becomes associated if $\zeta = 1$ and $n_q^p = 0$.

While the model has a large number of material constants, these are hierarchically structured in four groups. The most basic model implementation requires only group 1 (four parameters), while each additional group adds special optional features to the model (group 2 = nonlinear elasticity, group 3 = structure degradation, group 4 = volume dilatancy). As each group controls separate and independent features of the model, their calibration and evaluation are easier.

Constants a, c, σ_c, $m_{b,in}$ and d_{in} [$= (s_{in}/m_{b,in})\,\sigma_c$] control the initial shape and size of the Structure Envelope (SE) and can be determined from the peak strengths measured in several triaxial tests (at different confining pressures). Constants $m_{b,fin}$ and d_{fin} [$= (s_{fin}/m_{b,fin})\,\sigma_c$] control the magnitude of strain softening/hardening. Constants $\varepsilon_{q,f1}^p$ and $\varepsilon_{q,f2}^p$ are the accumulated plastic shear strains when post-failure strength reaches its residual value. Constant $\boldsymbol{b}$ controls peak strength in tension versus compression (classical HB assumes $\boldsymbol{b} = 0$). Constant c controls peak strength anisotropy at various loading directions (classical HB assumes $c = 1$). Constants (ξ_{in}, θ_{in}), $(\xi_{fin}, \theta_{fin})$, (ξ_0, θ_0),

n and γ can be determined from loading–unloading stress–strain curves in the pre-peak domain (Yoshinaka et al. 1996; Ribacchi 2000; Filimonov et al. 2001). In the absence of such data, constants $(\xi_{fin}, \theta_{fin})$ and (ξ_0, θ_0) can take values equal to about 20% and 80% of the corresponding initial values (ξ_{in}, θ_{in}) while $n = 0.5$ and $\gamma = 1$. Finally, dilatancy constants $(\zeta, n_q{}^p)$ can be calibrated by matching the $\varepsilon_{vol} - \varepsilon_a$ (volumetric vs. axial strain) response in triaxial or unconfined compression tests. Parameter ζ controls the gradient of the curve at first plastic loading, while the exponential parameter n_q^p controls the degradation rate to a quasi-critical state, where the specimen deforms without further volume change; classical HB dilatancy uses $\zeta = 1$ and $n_q{}^p = 0$.

7 Application of the SDR Model

The SDR model was implemented in the Finite Element Code Simulia ABAQUS and was applied in the one-dimensional (plane strain and axisymmetric) excavation of a long circular tunnel (radius $R = 5$ m) in an isotropic initial stress field ($p_0 = 2.5$ MPa, $K_o = 1$). The problem includes gradual reduction of the internal pressure (p) from the initial value (p_0) up to zero (full tunnel excavation) and comparison of the resulting convergence (u_R)–confinement (p) curves.

Figure 5 investigates the effect of stress–strain non-linearity on the predicted wall convergence (u_R)–confinement (p) curves. Figure 5a compares the linear and non-linear stress–strain curves used in the analyses. For simplicity, both cases have perfectly plastic response in the post-peak domain. As the linear curve matches the initial stiffness of the nonlinear curve, the tunnel wall convergence (u_R) in the NL case is significantly higher than that in the L case (Fig. 5b). Figure 5c shows similar behaviour for the radial convergence (u_r) at various distances (r) from the tunnel axis at full tunnel excavation ($p = 0$).
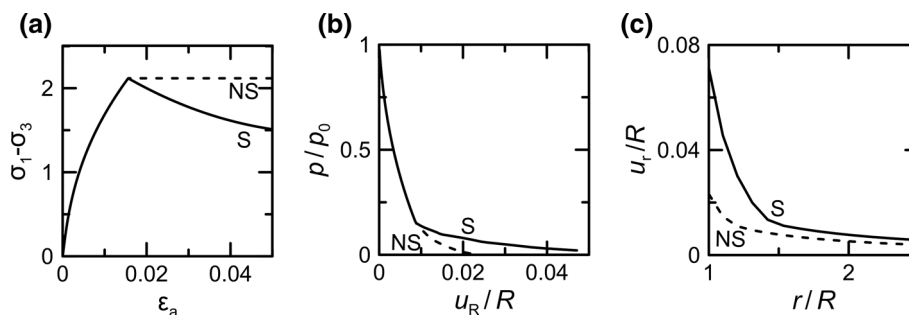
Fig. 6 Effect of post-peak strain softening (S—post-peak strain softening; NS—non-linear elastic-perfectly plastic response) on the convergence (u_R)–confinement (p) curve of tunnel excavation: **a** Drained triaxial shear stress ($\sigma_1-\sigma_3$) versus axial strain (ε_a) curves used in the analyses. **b** convergence (u_R)–confinement (p) curves and **c** radial convergence (u_r) versus distance (r) from the tunnel axis at full tunnel excavation ($p = 0$)

Figure 6 shows the effect of post-peak strain softening on the predicted tunnel wall convergence (u_R)–confinement (p) curves. Figure 6a compares the strain softening response (S) to its perfectly plastic-counterpart (NS) in the shear stress ($\sigma_1 - \sigma_3$) versus axial strain (ε_a) diagram of a drained triaxial test used in the analyses. Non-linear pre-peak response is the same in both cases. In the post-peak domain, the S case uses $d_{fin} = 0.5\ d_{in}$ and $m_{b,fin} = 0.5\ m_{b,in}$ (at $\varepsilon^p_{q,f1=2} = 0.08$). Strain softening causes appreciably larger convergence (Fig. 6b, c).

Figure 7 shows the effect of plastic volume dilatancy parameter (n^p_q) on the predicted convergence (u)–confinement (p) curves. For simplicity, the other dilatancy parameter is set to $\zeta = 1$ in both cases. Case D uses an associated flow rule ($n^p_q = 0$) giving relatively high dilatancy, since the plastic strain vector remains normal to the SE. Case VD uses a more realistic non-associated flow rule ($n^p_q = 50$) with dilatancy starting from the same initial value as the D case, but eventually reducing to zero at large shear strains (Fig. 7c). The high dilatancy case (D) predicts appreciably larger convergences, because the unrealistic volume increase at large strains requires an appreciable inward tunnel wall movement to be accommodated. In the case of a real tunnel, case (D) predicts much larger pressures of the tunnel lining, as the presence of the tunnel lining resists the evolution of inward wall movements by developing significant compression in the lining.

The SDR model uses a non-associated flow rule (which gives a non-positive definite stiffness matrix) and permits strain softening (which can make the problem ill-posed and lead to strain localisation in certain cases). Despite that, the numerical algorithm converged to a unique solution, largely independent of the mesh size (unless very coarse meshes were used), in all model applications so far, indicating that the model is relatively stable and accurate at least in these problems. To illustrate that, the SDR model was applied in the two-dimensional (plane strain)
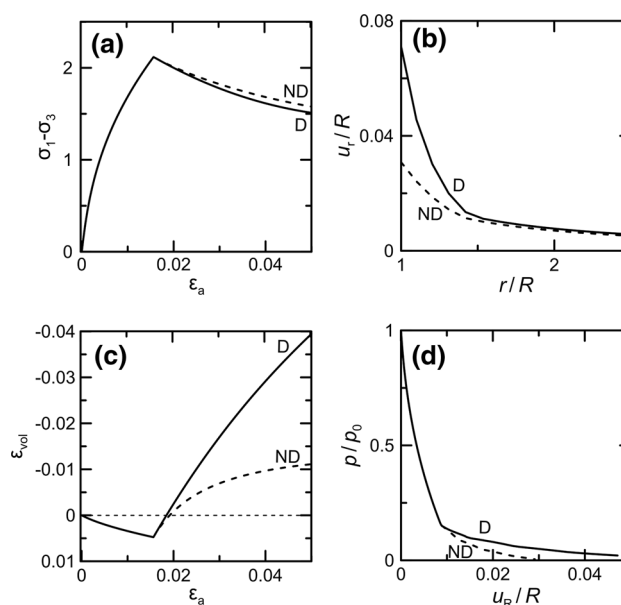

Fig. 7 Effect of post-peak volume dilatancy (D—associated dilatancy; VD—non-associated dilatancy) on the convergence (u_R)–confinement (p) curve of tunnel excavation: **a**, **c** Drained triaxial shear stress ($\sigma_1 - \sigma_3$) versus axial strain (ε_a) and volumetric strain (ε_{vol}) versus axial strain (ε_a) curves used in the analyses. **b** Radial convergence (u_r) versus distance (r) from the tunnel axis at full tunnel excavation ($p = 0$). **d** Convergence (u_R)–confinement (p) curves

excavation of a long circular tunnel (radius $R = 5$ m) in an anisotropic initial stress field ($p_0 = 2.5 MPa$, $K_o = 0.5$), using three mesh sizes: a fine (F) mesh with 11,520 elements, a coarse (C) mesh with 5978 elements and a very coarse (VC) mesh with only 960 elements. The lateral mesh boundaries were placed at distance $20R$ (=100 m) from the tunnel axis to minimise any influence of the boundaries. Boundary conditions included full restrain (pinning) at the bottom and horizontal restrain at both lateral boundaries. The problem included gradual reduction (up to zero) of the stiffness of the finite elements inside the
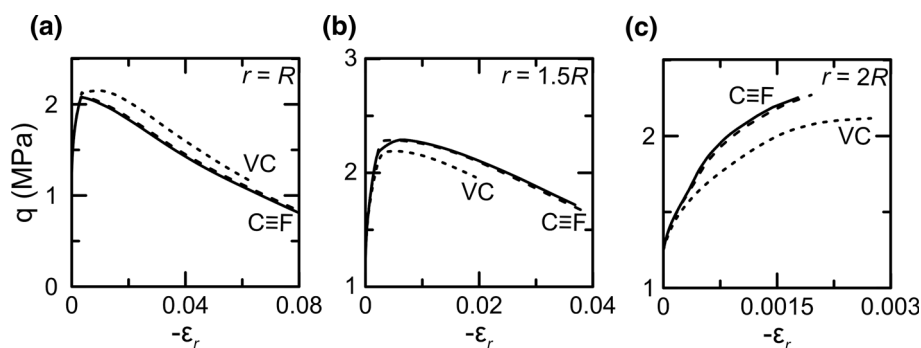
Fig. 8 Investigation of finite element mesh dependency on the shear stress (q)–radial strain (ε_r) curves at three points (along the tunnel springline) located at distances: **a** $r = R$ (tunnel wall), **b** $r = 1.5R$ and **c** $r = 2R$. The dashed line of the coarse mesh (C) and the solid line of the fine (F) mesh give practically identical results, while the very coarse mesh (VC) deviates significantly

tunnel and observation of the evolution of shear stress (q) versus radial strain (ε_r) curves at three points along the tunnel springline (located at distances $r = R$, $1.5R$ and $2R$ from the tunnel axis).

Figure 8 investigates the finite element mesh dependency with all adverse features of the model activated (non-linear and irreversible "elasticity", strongly non-associated flow rule and intense strain softening). The coarse (C) and fine (F) meshes give practically identical response, without any indication of incipient bifurcation, despite the significant strain softening close to the tunnel wall (at distances $r = R$ and $1.5R$). The very coarse (VC) mesh still converges to a unique but different solution, due to the very small number of finite elements.

8 Conclusions

The paper describes a continuum, incremental plasticity, rate-independent, constitutive model (SDR) applicable in weak rocks and heavily fractured rockmasses, where mechanical behaviour is controlled by rockmass strength rather than structural features (discontinuities). The SDR model is based on the Generalised Hoek–Brown (HB) failure criterion, has non-linear pre-peak stiffness to improve behaviour at small strains and under stress reversals (cyclic loading), uses Structure Degradation (damage) mechanisms to describe strain hardening (ductile) and strain softening (brittle) behaviour in the post-peak strength domain and implements a non-associated flow rule to improve volume dilatancy predictions especially at large shear strains (where dilatancy becomes negligible).

The model describes structure by a HB-type, curved, pressure-dependent Structure Envelope (SE) in the stress space which evolves with plastic strains. Stress paths inside the SE are non-linear and irreversible but do not modify material structure (no change of the SE), while stress paths

on the SE cause plastic strains and modify material structure. A stress point on the SE may tend to move towards the exterior of the SE (strain hardening) or towards the interior of the SE by pulling the SE with it (strain softening) or by retreating from the SE (non-plastic/unloading path).

The most general implementation of the model (with all features activated) requires 20 material constants which control nonlinear elasticity (8 constants), structure and its evolution (10 constants) and plastic dilatancy (2 constants), but more basic implementations with as few as four material constants are also possible (in the case of the classical generalised HB criterion). As each set of constants controls different aspects of the model, calibration is relatively straightforward.

The SDR model was implemented in the Finite Element Code Simulia ABAQUS and was applied in: (a) the one-dimensional (plane strain and axisymmetric) excavation of a long circular tunnel in an isotropic initial stress field and (b) the two-dimensional (plane strain) excavation of the same tunnel in an anisotropic initial stress field ($K_o = 0.50$). Both cases modelled gradual tunnel excavation by a gradual stiffness reduction of the finite elements inside the tunnel and compared the resulting convergence (u_R)–confinement (p) and shear stress (q)–radial strain (ε_r) curves. It is shown that non-linear and irreversible pre-peak response, hardening/softening characteristics and variable volume dilatancy have significant influence on the predicted response. Investigation of finite element mesh dependency with all adverse features of the model activated (non-linear and irreversible "elasticity", strongly non-associated flow rule and intense strain softening) shows invariance on the mesh size (with the exception of very coarse meshes) without any indication of incipient bifurcation.

References

Al-Ajmi AM, Zimmerman RW (2005) Relation between the Mogi and the Coulomb failure criteria. Int J Rock Mech Min Sci 42:431–439

Alejano L, Alonso E (2005) Considerations of the dilatancy angle in rocks and rock masses. Int J Rock Mech Min Sci 42:481–507

Alejano L, Garcia Bastante F, Alonso E, Taboada J (1999) Back analysis of a rock-burst in a shallow room and pillar gypsum exploitation. In: 9th ISRM congress, Paris, pp 1077–1080

Chang C, Haimson B (2000) True triaxial strength and deformability of the German Continental Deep Drilling Program (KTB) deep hole amphibolite. J Geophys Res Solid Earth 105:18999–19013

Crouch S (1970) Experimental determination of volumetric strains in failed rock. Int J Rock Mech Min Sci Geomech Abstr 7(6):589–603

Detournay E (1986) Elastoplastic model of a deep tunnel for a rock with variable dilatancy. Rock Mech Rock Eng 19:99–108

Filimonov YL, Lavrov AV, Shafarenko YM, Shkuratnik VL (2001) Memory effects in rock salt under triaxial stress state and their use for stress measurement in a rock mass. Rock Mech Rock Eng 34:275–291

Frantziskonis G, Desai C (1988) Constitutive model with strain softening. Math Comput Model 10:794

Gerogiannopoulos N, Brown E (1978) The critical state concept applied to rock. Int J Rock Mech Min Sci Geomech Abstr 15(1):1–10

Hill R (1958) A general theory of uniqueness and stability in elastic-plastic solids. J Mech Phys Solids 6:236–249

Hoek E (1983) Strength of jointed rock masses. Geotechnique 33:187–223

Hoek E, Brown ET (1980) Empirical strength criterion for rock masses. J Geotech Eng Div 106(9):1013–1035

Hoek E, Brown E (1997) Practical estimates of rock mass strength. Int J Rock Mech Min Sci 34:1165–1186

Hoek E, Diederichs M (2006) Empirical estimation of rock mass modulus. Int J Rock Mech Min Sci 43:203–215

Hoek E, Wood D, Shah S (1992) A modified Hoek–Brown criterion for jointed rock masses. In: Proceedings of the rock characterization, symposium on international society of rock mechanics: Eurock, pp 209–214

Hoek E, Kaiser P, Bawden W (1995) Support of underground excavations in hard rock. AA Balkema, Rotterdam

Hoek E, Carranza-Torres C, Corkum B (2002) Hoek–Brown failure criterion-2002 edition. In: Proceedings of NARMS-TAC, pp 267–273

Kavvadas M, Amorosi A (2000) A constitutive model for structured soils. Geotechnique 50:263–273

Kudoh K, Koyama T, Nambu S, Suzuki Y, Ishibashi K (1999) Support design of a large underground cavern considering strain-softening of rock. In: 9th ISRM congress, International Society for Rock Mechanics

Ma L-J, Liu X-Y, Wang M-Y, Xu H-F, Hua R-P, Fan P-X, Jiang S-R, Wang G-A, Yi Q-K (2013) Experimental investigation of the mechanical properties of rock salt under triaxial cyclic loading. Int J Rock Mech Min Sci 62:34–41

Mandel J (1966) Conditions de stabilité et postulat de Drucker. In: Rheology and Soil Mechanics/Rhéologie et Mécanique des Sols, Springer

Mas Ivars DM, Pierce ME, Darcel C, Reyes-Montes J, Potyondy DO, Paul Young R, Cundall PA (2011) The synthetic rock mass approach for jointed rock mass modelling. Int J Rock Mech Min Sci 48:219–244

Medhurst T, Brown E (1998) A study of the mechanical behaviour of coal for pillar design. Int J Rock Mech Min Sci 35:1087–1105

Mogi K (1971) Fracture and flow of rocks under high triaxial compression. J Geophys Res 76:1255–1269

Mroz Z (1963) Non-associated flow laws in plasticity. J Mécanique 2:21–42

Pan X, Hudson J (1988) A simplified three dimensional Hoek–Brown yield criterion. In: ISRM international symposium, International Society for Rock Mechanics

Priest S (2005) Determination of shear strength and three-dimensional yield strength for the Hoek–Brown criterion. Rock Mech Rock Eng 38:299–327

Ribacchi R (2000) Mechanical tests on pervasively jointed rock material: insight into rock mass behaviour. Rock Mech Rock Eng 33:243–266

Wang R, Kemeny J (1995) A new empirical failure criterion for rock under polyaxial compressive stresses. In: The 35th US symposium on rock mechanics (USRMS), American Rock Mechanics Association

Wang Z-L, Li Y-C, Wang J (2007) A damage-softening statistical constitutive model considering rock residual strength. Comput Geosci 33:1–9

Wang S, Zheng H, Li C, Ge X (2011) A finite element implementation of strain-softening rock mass. Int J Rock Mech Min Sci 48:67–76

Yoshinaka R, Osada M, Tran TV (1996) Deformation behaviour of soft rocks during consolidated-undrained cyclic triaxial testing. Int J Rock Mech Min Sci Geomech Abstr 33:557–572

Yuan S-C, Harrison J (2004) An empirical dilatancy index for the dilatant deformation of rock. Int J Rock Mech Min Sci 41:679–686